JBC RESEARCH ARTICLE

Degradation of the *E. coli* antitoxin MqsA by the proteolytic complex ClpXP is regulated by zinc occupancy and oxidation

Received for publication, July 13, 2021, and in revised form, December 24, 2021 Published, Papers in Press, December 30, 2021,
https://doi.org/10.1016/j.jbc.2021.101557

Margaret R. Vos[1,2,‡], Benjamin Piraino[3,‡], Christopher J. LaBreck[3], Negar Rahmani[3], Catherine E. Trebino[3], Marta Schoenle[4], Wolfgang Peti[5], Jodi L. Camberg[3,*], and Rebecca Page[1,*]

From the [1]Department of Cell Biology, and [2]Graduate Program in Molecular Biology and Biochemistry, University of Connecticut Health Center, Farmington, Connecticut, USA; [3]Department of Cell & Molecular Biology, The University of Rhode Island, Kingston, Rhode Island, USA; [4]Department of Chemistry and Biochemistry, University of Arizona, Tucson, Arizona, USA; [5]Department of Molecular Biology and Biophysics, University of Connecticut Health Center, Farmington, Connecticut, USA

Edited by Karen Fleming

It is well established that the antitoxins of toxin–antitoxin (TA) systems are selectively degraded by bacterial proteases in response to stress. However, how distinct stressors result in the selective degradation of specific antitoxins remain unanswered. MqsRA is a TA system activated by various stresses, including oxidation. Here, we reconstituted the *Escherichia coli* ClpXP proteolytic machinery *in vitro* to monitor degradation of MqsRA TA components. We show that the MqsA antitoxin is a ClpXP proteolysis substrate, and that its degradation is regulated by both zinc occupancy in MqsA and MqsR toxin binding. Using NMR chemical shift perturbation mapping, we show that MqsA is targeted directly to ClpXP *via* the ClpX substrate targeting N-domain, and ClpX mutations that disrupt N-domain binding inhibit ClpXP-mediated degradation *in vitro*. Finally, we discovered that MqsA contains a cryptic N-domain recognition sequence that is accessible only in the absence of zinc and MqsR toxin, both of which stabilize the MqsA fold. This recognition sequence is transplantable and sufficient to target a fusion protein for degradation *in vitro* and *in vivo*. Based on these results, we propose a model in which stress selectively targets nascent and zinc-free MqsA, resulting in exposure of the ClpX recognition motif for ClpXP-mediated degradation.

Bacterial toxin–antitoxin (TA) modules are ubiquitous genetic elements that code for a toxin capable of inhibiting bacterial growth and a cognate antitoxin that binds and inhibits toxin activity (1–4). For more than a decade, it has been hypothesized that TA systems play a key role in bacterial persistence, a phenotypic state of bacteria characterized by growth arrest and increased resistance to antibiotics. Consistent with this hypothesis, multiple studies have confirmed links between TA systems and persistence, including gene expression profiling experiments that identified TA toxins as the most highly upregulated genes in isolated *Escherichia coli* persister cells (5–7). However, recent work has shown that, under the conditions tested, deleting the TA systems in *E. coli* does not significantly contribute to bacterial fitness, even upon exposure to stress, suggesting that the presence of TA systems may not significantly promote survival (8–10). Despite their prevalence throughout the bacterial kingdom, the endogenous roles of TA systems and how they contribute to bacterial fitness are still poorly understood.

Although the biological functions of TA systems remain elusive, how they function and are regulated at a molecular level is well established (1, 11–13). Type II TA systems constitute the largest family of TA systems and are comprised of a two-gene operon that encodes a labile protein antitoxin and a stable protein toxin. Under normal conditions, the TA forms a stable complex, which inhibits toxin activity. However, under conditions of stress, such as nutrient starvation or oxidative stress, antitoxins are rapidly degraded by cellular proteases, especially Lon and ClpXP (10, 14–20). This results in an increase of the TA ratio in the cell, eventually resulting in free toxin, which can then act on its substrates and arrest cell growth, for example, by cleaving mRNA (many toxins are RNases (1)). Despite these advances, a molecular understanding of how the likely highly specific cellular stressors target distinct antitoxins for degradation remains an open question.

MqsRA is an *E. coli* TA system that can be activated by oxidative stress (21). The *mqsR* gene encodes a 98-amino acid sequence–specific mRNA endoribonuclease from the RelE family of bacterial toxins (Fig. 1, *A* and *B*) (11, 22, 23). Immediately downstream of *mqsR* is *mqsA*, which encodes the 131-amino acid cognate antitoxin of MqsR and also binds the *mqsRA* operon to repress its transcription. MqsA binds and neutralizes MqsR toxicity *via* its N-terminal domain (Fig. 1, *A* and *B*) (11, 24). The selective degradation of MqsA in response to stress by the major bacterial proteases Lon and ClpXP (10, 21) results in excess MqsR toxin, which is then free to degrade the cellular mRNA pool at GCU/A sequences, and, in turn, halt translation and induce growth arrest (11, 22). However, unlike most antitoxins, MqsA is not an intrinsically disordered protein (IDP) in the absence of its cognate toxin, a structural feature hypothesized to contribute

‡ These authors contributed equally to this work.
* For correspondence: Jodi L. Camberg, cambergj@uri.edu; Rebecca Page, rpage@uchc.edu.

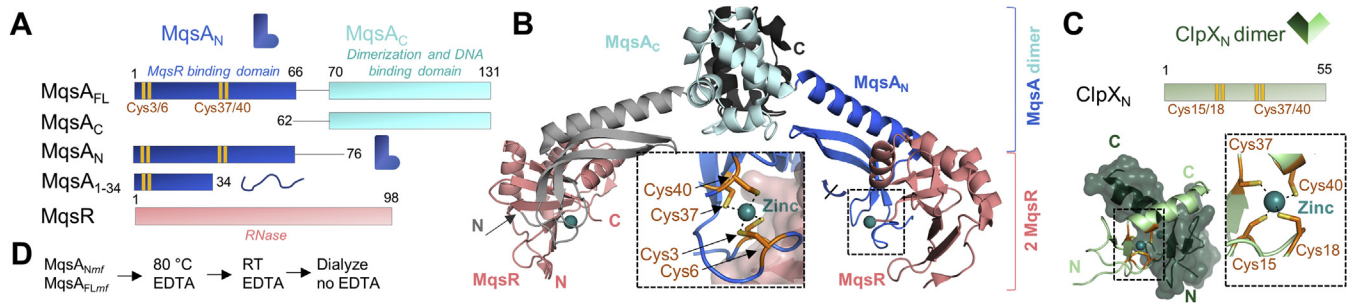

Figure 1. ClpX$_N$ and MqsRA. *A*, MqsA and MqsR constructs used in this study. The MqsR toxin is a single domain ribonuclease. The MqsA antitoxin is a two-domain protein (MqsA$_N$ and MqsA$_C$). MqsR binds MqsA$_N$, and this is the domain that also binds zinc *via* four cysteine residues (Cys3, Cys6, Cys37, and Cys40). The C-terminal dimerization domain binds DNA. *B*, model of the MqsA (*grays*, *blues*; Protein Data Bank [PDB]: 3GN5) bound to MqsR (*coral*; PDB: 3HI2) based on the structures of the MqsA dimer and the MqsA$_N$–MqsR complex. The *inset* shows the zinc coordination site, with the coordinating cysteine residues shown as *sticks* in *orange*. *C*, ClpX N-terminal zinc-binding domain (ClpX$_N$) is a dimer (one monomer, *dark green surface*; second monomer, *light green ribbon*; PDB: 2DS6). Zinc-binding cysteine residues (Cys15, Cys18, Cys37, and Cys40) are shown as *sticks* in *orange*, with the zinc ion in *teal*. *D*, preparation of metal-free (mf) MqsA$_{FLmf}$ and MqsA$_{Nmf}$. MqsA$_C$, C-terminal domain of MqsA; MqsA$_N$, N-terminal domain of MqsA.

to the ability of antitoxins to be rapidly degraded by bacterial proteases. Rather, MqsA is fully structured in the absence of bound toxin, stabilized, in part, by a zinc ion that is coordinated by four cysteine residues in its N-terminal MqsR-binding domain (Fig. 1*B*).

To understand how, at a molecular level, MqsA is targeted for degradation by bacterial proteases and to advance our understanding of how substrates are recognized by bacterial proteolytic systems, especially ClpXP, we studied the mechanism of MqsA recognition and degradation by the ClpXP protease. The two-component ClpXP proteosome consists of hexamers of ClpX, which is a member of the AAA+ family of proteins, bound to one or both sides of a barrel-shaped ClpP complex (25). ClpP is a serine protease that assembles as a face-to-face dimer of heptameric rings, creating an internal proteolytic chamber. Protein turnover is initiated when a substrate is recognized by ClpX either directly or through a secondary adaptor protein. Thus, substrate is processively unfolded by ClpX in a series of ATP-dependent power strokes as the substrate polypeptide chain is translocated through the central channel and into the ClpP proteolytic chamber for degradation (26). Previous work showed that MqsA is a substrate of ClpXP. Here, we show that MqsA is efficiently degraded by ClpXP in the absence of zinc, and that both zinc and MqsR binding antagonize ClpXP-mediated degradation. Furthermore, we used biomolecular NMR-based chemical shift perturbation (CSP) experiments to show that folded and metal-bound MqsA does not interact with the ClpX N-domain (a small recognition domain that binds a subset of ClpXP substrates and adaptor proteins, Fig. 1*C*) but instead ClpX$_N$ only interacts with unfolded and metal-free MqsA. Finally, we also show that the MqsA-binding site on the ClpX N-domain overlaps with, but is not identical to, the binding pocket for the SspB adaptor protein (27). In addition to the *in vitro* assays, we also successfully showed that, *in vivo*, turnover of a fusion protein containing the MqsA recognition sequence is diminished in the absence of the ClpXP protease. We propose a model in which stress, such as oxidation, renders nascent MqsA unable to fold, resulting in its selective degradation by ClpXP and the activation of the MqsR toxin.

Results

Zinc and MqsR protect MqsA from degradation by ClpXP

Using purified *E. coli* ClpX and ClpP, we reconstituted active proteasomes *in vitro* to monitor degradation of MqsRA proteins. We purified MqsA, with and without a bound zinc (Fig. 1, *A*, *B*, and *D*). MqsA$_{FL}$ (full-length) and MqsA$_{FLmf}$ (metal-free) were incubated individually and together. ClpXP and ATP were then added, and the reactions incubated for 1 h. MqsA degradation was monitored over time by SDS-PAGE (Fig. 2*A*). We observed that MqsA$_{FLmf}$ is rapidly degraded, with most of the protein proteolyzed after 20 min; however, under the same conditions, MqsA$_{FL}$ is not degraded. This suggests that zinc coordination stabilizes MqsA against ClpXP degradation. Next, we tested if MqsA$_{FLmf}$ degradation is modified by MqsR, since together MqsA and MqsR form the hetero-oligomeric MqsRA complex (Fig. 2*B*). Our results indicate that MqsR, *via* complex formation with MqsA, antagonizes MqsA degradation, and MqsR does not antagonize degradation of another ClpXP proteolysis substrate, Gfp fused to the ssrA tag sequence (Gfp-ssrA) (Fig. S1*A*). Together, these data show that MqsA is degraded by ClpXP, with both zinc binding and MqsR binding protecting MqsA against degradation by ClpXP. These data further show that ClpXP-mediated degradation of MqsA does not require an adaptor protein, as no adaptor protein was present in these assays.

ClpXP targeting is mediated by the MqsA N-terminal domain

The ability of zinc and MqsR to protect MqsA against ClpXP-mediated degradation suggests that ClpXP engages MqsA *via* its N-terminal zinc-binding and MqsR-binding domain. To test this, the N-terminal and C-terminal domains of MqsA (MqsA$_{Nmf}$ [residues 1–76]; MqsA$_C$ [residues 62–131]; Fig. 1, *A* and *B*) were prepared and tested for their ability to be degraded by ClpXP. The data show that only MqsA$_{Nmf}$ is degraded by ClpXP; MqsA$_C$ is not (Fig. 2*C*).

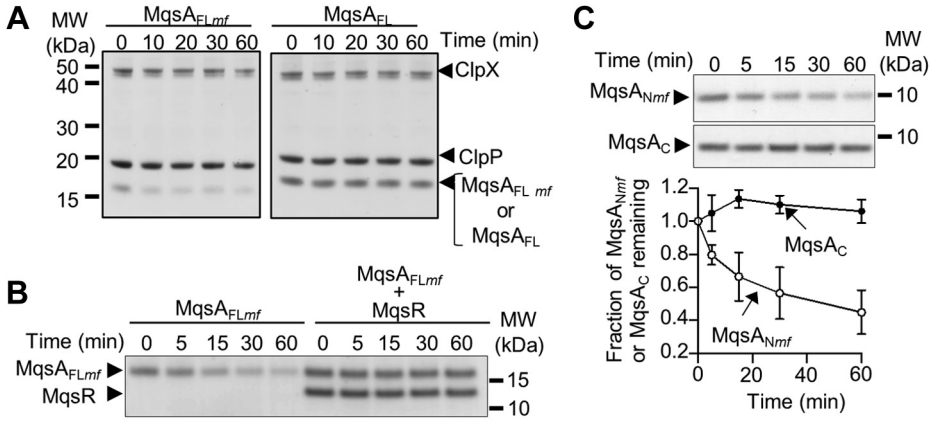

Figure 2. The degradation of MqsA by ClpX is inhibited by MqsR and zinc. *A*, degradation reactions containing ClpX (1 μM), ClpP (1 μM), ATP (5 mM), and an ATP-regenerating system with MqsA$_{FL}$ (6 μM) or MqsA$_{FLmf}$ (6 μM), where indicated. Samples were taken at 0, 10, 20, 30, and 60 min and analyzed by SDS-PAGE and Coomassie staining. *B*, time course of MqsA$_{FLmf}$ (4 μM) degradation in the presence and absence of MqsR (4 μM; added prior to ClpXP) with ClpX (0.5 μM), ClpP (0.6 μM), ATP, and an ATP-regenerating system. Samples were taken at 0, 5, 15, 30, and 60 min and analyzed by SDS-PAGE and Coomassie staining. *C*, time course of MqsA$_{Nmf}$ (6 μM) (*open circles*) and MqsA$_C$ (6 μM) (*closed circles*) degradation with ClpX (1 μM), ClpP (1 μM), ATP, and an ATP-regenerating system. Band intensity was measured by densitometry, and error is reported a as standard deviation. *A–C*, reactions shown are representative of at least three independent replicates. MqsA$_C$, C-terminal domain of MqsA; MqsA$_N$, N-terminal domain of MqsA.

Similar to MqsA$_{FLmf}$ (Fig. 2, *A* and *B*), the majority of MqsA$_{Nmf}$ is degraded in approximately 20 min. This highlights that MqsA residues required for targeting MqsA to ClpX are located within the first 76 residues of MqsA (Fig. 2*C*).

Metal-loaded MqsA$_N$ does not bind ClpX$_N$

The N-domain of ClpX interacts directly with some substrates, such as UmuD′, Lambda O protein, MuA and FtsZ, and substrate-specific adaptor proteins, such as SspB (27–32). Here, we observed that the ClpX N-domain (ClpX$_N$; amino acids 1–55) forms a homodimer that, like MqsA$_N$, binds zinc *via* four cysteines (Cys15, Cys18, Cys37, and Cys40; Fig. 1*C*), which is consistent with previous reports (27, 33). In order to determine how MqsA$_N$ and ClpX$_N$ interact at a molecular level, we used NMR CSP mapping, in which the changes in the chemical shifts of ^{15}N-labeled protein are used to identify the residues that constitute a ligand-binding and/or protein-binding site. We first tested the importance of zinc for ClpX$_N$ structure by comparing the 2D [^{1}H, ^{15}N] heteronuclear single quantum coherence (HSQC) spectra of ClpX$_N$ in the absence and presence of zinc. The spectrum quality improves substantially in the presence of excess zinc, showing that zinc is necessary for ClpX$_N$ folding and stability (Fig. S1*B*); thus, zinc was included in all subsequent ClpX$_N$ experiments. CSP mapping was then used to determine if the MqsA$_N$ interacts with ClpX$_N$. No CSPs were observed in ^{15}N-labeled ClpX$_N$ in the presence of 10-fold molar excess of MqsA$_N$ (Fig. 3*A*). These data demonstrate that metal-loaded MqsA$_N$ does not bind ClpX$_N$, an observation consistent with the data that show that metal-loaded MqsA is resistant to ClpXP-mediated degradation (Fig. 2*A*).

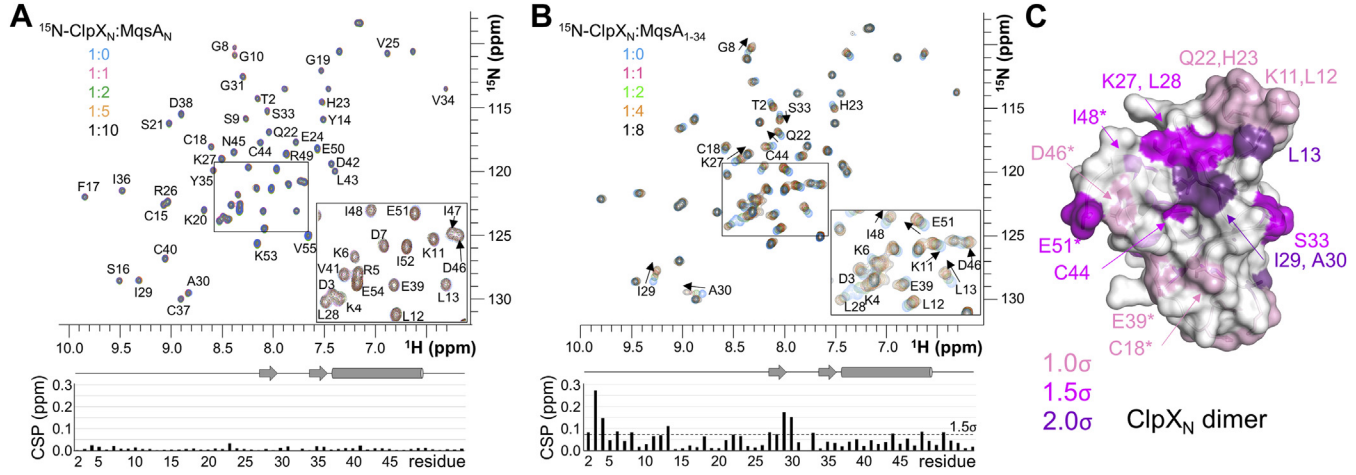

Figure 3. ClpX$_N$ only binds MqsA$_N$ when it is unfolded and does not coordinate zinc. *A*, overlay of 2D [^{15}N, ^{1}H] HSQC spectra of ^{15}N-labeled ClpX$_N$ in the presence of increasing concentrations of MqsA$_N$. CSPs *versus* residue numbers are shown below. No significant CSPs are observed. *B*, overlay of 2D [^{15}N, ^{1}H] spectra of ^{15}N-labeled ClpX$_N$ in the presence of increasing concentrations of MqsA$_{1–34}$, which cannot bind zinc and is unfolded. Multiple CSPs are observed. CSPs *versus* residue numbers are shown below; 1.5σ level is indicated by a *dashed line*. *C*, residues that experience significant CSPs are plotted on the surface of the ClpX$_N$ crystal structure (PDB: 2DS6) and highlighted in *pink* (≥1σ), *magenta* (≥1.5σ), and *purple* (≥2.0σ) (* indicates residues from chain B of the dimer). CSP, chemical shift perturbation; HSQC, heteronuclear single quantum coherence; MqsA$_N$, N-terminal domain of MqsA.

Unfolded and metal-free MqsA binds $ClpX_N$

Because the K_D of $MqsA_N$ for zinc is estimated to be $<10^{-15}$ M (34), the zinc present in the $ClpX_N$ buffer ensures that MqsA is fully metal loaded, even if initially prepared as metal free (Fig. 1*D*). Thus, in order to study a WT variant that was unable to bind zinc, we generated an $MqsA_N$ deletion that lacks two of the four Cys residues required for zinc binding (Fig. 1*A*; residues 1–34, $MqsA_{1-34}$, includes only Cys3 and Cys6). The 2D [^{1}H, ^{15}N] HSQC of $MqsA_{1-34}$ confirmed that $MqsA_{1-34}$ is unfolded independent of the presence of zinc (Fig. S2*A*; compare also with the 2D [^{1}H, ^{15}N] HSQC spectrum of folded $MqsA_N$; Fig. S2*B*). We then completed the sequence-specific backbone assignment of $ClpX_N$ in order to probe the interaction of $MqsA_{1-34}$ with ^{15}N-labeled $ClpX_N$ at four $ClpX_N$:$MqsA_{1-34}$ ratios (1:1; 1:2; 1:4; and 1:8). Upon the addition of $MqsA_{1-34}$, 17 CSPs were observed in ^{15}N-labeled $ClpX_N$ (>1.5σ), with the strongest CSPs observed for residues Asp3, Lys4, Leu13, Lys27, Ile29, and Ala30 (Fig. 3, *B* and *C*). To confirm that the interaction is specific for $MqsA_{1-34}$, and not because it is an IDP, we performed CSP experiments with two distinct and well-characterized IDPs: $PNUTS_{376-435}$ or inhibitor-2 (Fig. S3). No significant CSPs in ^{15}N-labeled $ClpX_N$ were observed when titrated with either $PNUTS_{376-435}$ and Inhibitor-2_{10-165}, demonstrating that the MqsA interaction is specific. Together, these data show that $ClpX_N$ binds directly and specifically to residues within the first 34 amino acids of MqsA.

Identification of the $MqsA_N$ motif recognized by ClpX

To identify the MqsA residues that bind $ClpX_N$, we performed reverse CSP experiments. After completing the sequence-specific backbone assignment of $MqsA_{1-34}$, increasing concentrations of $ClpX_N$ were added to ^{15}N-labeled $MqsA_{1-34}$ and the resulting CSPs identified. Seven residues experienced significant CSPs (>1.5σ): Ile18, Thr21, Phe22, Gly24, Leu29, Ile32, and Gly34, with one peak, Gly31, broadened beyond detection (Fig. 4). Most of these residues are buried in the hydrophobic core of folded MqsA, with Phe22, Leu29, and Ile32 being nearly completely buried from solvent (percent of solvent accessibility in folded MqsA: 20.8, 3.6, and 4.1, respectively). These data identify the MqsA residues that mediate $ClpX_N$ recognition and explain why folded $MqsA_N$, in which these residues are buried in the hydrophobic core, are unable to bind $ClpX_N$.

$MqsA_{1-34}$ contains a transplantable degron, the MqsA degron, for ClpXP

To determine if an $MqsA_{1-34}$ peptide sequence is capable of independently targeting a protein for degradation, we produced a chimeric fusion protein with Gfp fused to the N-terminus of $MqsA_{1-34}$ and measured degradation by monitoring loss of fluorescence after incubation with ClpXP *in vitro*. Gfp, without a specific ClpX degron, is not recognized or degraded by ClpXP (35); however, if $MqsA_{1-34}$ is recognized by ClpX, then we predict that ClpXP will unfold and degrade Gfp-$MqsA_{1-34}$, leading to a loss of Gfp fluorescence. In the absence

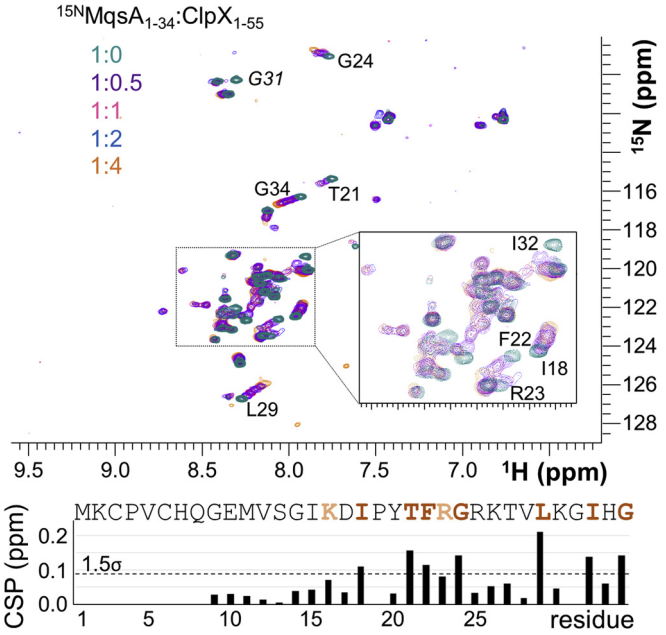

Figure 4. Residues on MqsA that bind to $ClpX_N$. Overlay of 2D [^{15}N, ^{1}H] HSQC spectra of ^{15}N-labeled $MqsA_{1-34}$ in the presence of increasing concentrations of $ClpX_N$. Multiple CSPs are observed. CSPs *versus* residue numbers are shown below; 1.5σ level is indicated by a *dashed line* (1.0σ, residue label in *beige*; ≥1.5σ, residue label in *brown*). CSP, chemical shift perturbation; HSQC, heteronuclear single quantum coherence.

of ClpXP, Gfp-$MqsA_{1-34}$ fluorescence is stable over time (Fig. 5*A*). In the presence of ClpXP, we observed a rapid loss of fluorescence, demonstrating that ClpX binds $MqsA_{1-34}$ resulting in Gfp-$MqsA_{1-34}$ unfolding and subsequent degradation by bound ClpP. Consistent with these data, we also showed that the turnover of Gfp-$MqsA_{1-34}$ is diminished in the ClpXP protease deletion strains (Fig. 5*B*). These data confirm that MqsA contains a cryptic N-domain recognition sequence, the MqsA degron, that is accessible only in the absence of zinc and MqsR toxin and that this recognition sequence is transplantable and sufficient to target a fusion protein (Gfp-$MqsA_{1-34}$) for degradation *in vitro* and *in vivo*.

We then confirmed the identity of the residues that define the $MqsA_{1-34}$ binding pocket on $ClpX_N$ using mutagenesis and fluorescence degradation assays. Specifically, we mutated $ClpX_N$ residues that (1) experienced CSPs upon titration with $MqsA_{1-34}$; (2) are solvent accessible; and (3) are unlikely to disrupt nearby regions upon mutagenesis (L12, L13, H23, and A30) (Fig. 3, *B* and *C*). We first confirmed that the engineered ClpX variants (ClpX[L13A], ClpX[L13D], ClpX[A30S], ClpX[L12S], and ClpX[H23A]) were properly folded and functional by showing (1) that the $ClpX_N$ variants were folded using ^{1}H 1D NMR spectroscopy; (2) that all full-length ClpX variants, like WT ClpX, purified as assembled hexamers by size-exclusion chromatography (SEC); (3) that the full-length ClpX variants hydrolyzed ATP; and (4) that the full-length ClpX variants complex with ClpP to degrade Gfp-ssrA, which bypasses the ClpX N-domain (Fig. S4). Next, ClpX variants were tested in degradation assays with ClpP and Gfp-$MqsA_{1-34}$. The data show that degradation for ClpX variant A30S was similar to WT ClpX, but degradation was

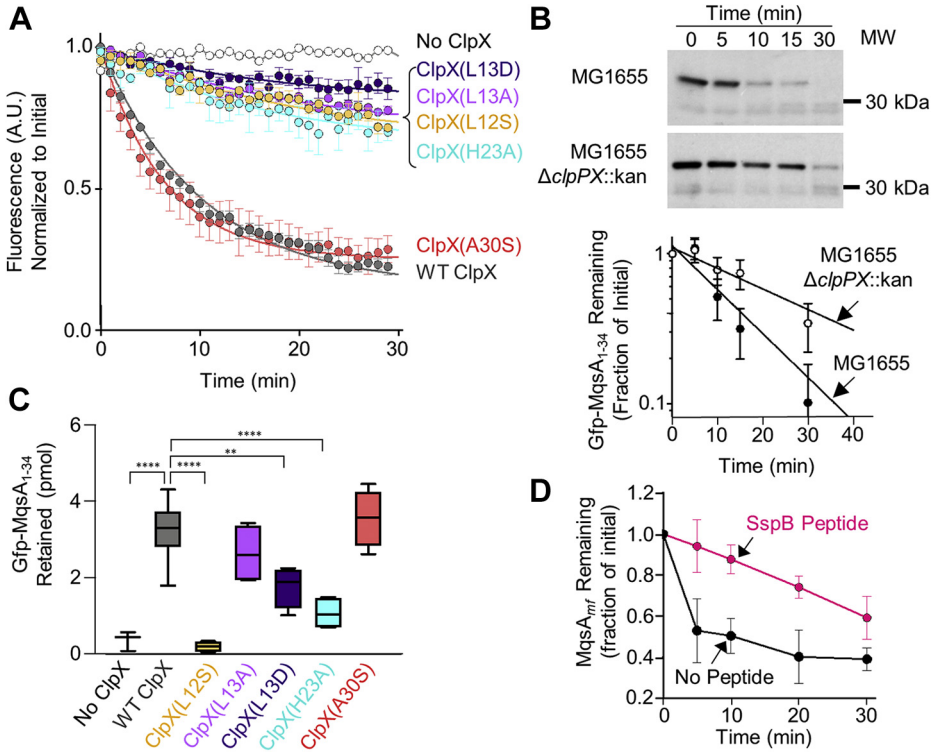

Figure 5. Substitution mutations in the ClpX N-domain impair MqsA degradation. *A*, Gfp-MqsA$_{1-34}$ (0.5 μM) degradation was monitored by measuring loss of fluorescence over time in reactions containing WT ClpX (*gray*) or ClpX N-domain variants ClpX(L12S) (*yellow*), ClpX(L13D) (*purple*), ClpX(L13A) (*lavender*), ClpX(H23A) (*aqua*), or ClpX(A30S) (*red*) (0.75 μM), where indicated, with ClpP (1.2 μM), ATP, and an ATP-regenerating system. *Curves* shown are an average of at least three replicates, and error is reported as a standard error. Degradation reactions shown are representative of at least three independent replicates. *B*, time course of Gfp-MqsA$_{1-34}$ protein turnover in cells, MG1655 WT, or MG1655 Δ*clpPX*::kan-expressing plasmid encoded Gfp-MqsA$_{1-34}$, where indicated, after addition of spectinomycin (200 μg/ml). Samples were taken at 0, 5, 10, 15, and 30 min, and total proteins were precipitated and analyzed by immunoblotting with anti-Gfp antibodies. Band intensity was measured by densitometry. Data are representative of at least three biological replicates, and standard error is shown. *C*, Gfp-MqsA$_{1-34}$ (3 μM) was incubated on ice with ClpX WT and N-domain variants (0.7 μM) in binding reactions containing ClpP (1.4 μM) and ATP. Stable complexes were collected by ultrafiltration and quantified by fluorescence. Data are represented as a box and whisker plot with the median value indicated by a horizontal line (****$p < 0.0001$; **$p < 0.005$). *D*, time course of MqsA$_{FLmf}$ (3 μM) degradation in reactions containing ClpX (0.5 μM), ClpP (0.6 μM), ATP, and an ATP-regenerating system in the absence and presence of the SspB peptide (150 μM), where indicated. Band intensity was measured by densitometry, and error is reported as standard error. *C* and *D*, degradation reactions shown are representative of at least three independent replicates.

significantly reduced for ClpX variants, L12S, L13A, L13D, and H23A (Fig. 5*A*). To confirm that the slower degradation rates observed were due to a reduction in MqsA$_{1-34}$ binding to ClpX, and not because of a defect in delivery or translocation through the ClpX pore, we used ClpXP filter retention assays. Consistent with the degradation results from ClpX variants, we observed that Gfp-MqsA$_{1-34}$ was retained by WT ClpX and ClpX A30S, but retention was defective for ClpX variants L12S, L13A, L13D, and H23A (Fig. 5*C*). Together, these results confirm that the region of the ClpX N-domain implicated in binding to MqsA by NMR is important for recognition and degradation by ClpXP.

The MqsA$_{1-34}$ binding pocket on ClpX$_N$ overlaps, but is not identical, to that of SspB

The amino acid residues in the ClpX N-domain implicated in MqsA recognition are close to or overlapping with residues, including H23, identified as important for binding to the C-terminus of the SspB adaptor protein. To determine if the SspB adaptor protein and MqsA use overlapping sites on the surface of ClpX, we tested if a peptide containing 11 C-terminal amino acid residues of SspB inhibits degradation of MqsA$_{mf}$; a similar peptide was previously shown to inhibit degradation of ssrA-tagged substrates in SspB adaptor–mediated degradation reactions (36). The data show that the C-terminal SspB peptide reduced MqsA$_{mf}$ degradation, confirming that the binding sites for SspB and MqsA on ClpX$_N$ overlap (Fig. 5*D*).

Discussion

Stress accelerates antitoxin turnover *via* regulated proteolysis (10, 14, 15, 20); however, a molecular understanding of how antitoxins are targeted for degradation by Lon and/or ClpXP remains an open question (10, 17–20, 37). Here, we show how the MqsA antitoxin, because of the presence of a novel cryptic MqsA degron that is only accessible in unfolded MqsA, is recognized and degraded by ClpXP. Specifically, we discovered, unexpectedly, that folded MqsA does not interact with ClpX$_N$, even with weak affinities. Consistent with this, folded MqsA is not degraded by ClpXP. Instead, we showed that ClpX$_N$ only binds MqsA when MqsA is unfolded. This led to the discovery of a cryptic ClpX$_N$ recognition motif

within the first 34 residues of MqsA that is buried when MqsA is folded but becomes accessible when MqsA is prevented from folding. Furthermore, we observed that the chimeric Gfp-MqsA$_{1-34}$ fusion protein, in which the MqsA remains flexible, is degraded by ClpXP *in vitro* and *in vivo* (Fig. 5*B*). Thus, the ClpX recognition motif of MqsA is transplantable, defining a novel ClpX degron, the MqsA degron, with an amino acid sequence that differs from all previously described degrons (38).

Because the MqsA degron is only accessible in unfolded MqsA, interactions that stabilize folded MqsA, such as zinc and/or MqsR binding, potently inhibit ClpXP-mediated MqsA degradation. These *in vitro* data are fully consistent with recent *in vivo* experiments showing that, in cells, both MqsA and a second antitoxin, YefM, are protected from degradation when bound to their cognate toxins (10, 20). By extension from our data, it is likely that the YefM toxin-binding domain also contains a degron that is accessible only in the absence of toxin. According to these structurally dependent events, this leads to the following question: under what conditions are MqsA (unfolded and cryptic ClpX$_N$ degron accessible) and YefM (not bound to toxin) susceptible to degradation? In the case of MqsA, actively translated and nascent MqsA is the likely target. This is because, during synthesis and prior to folding, the cryptic MqsA degron would be accessible. Alternatively, in oxidative conditions, the cysteines of nascent MqsA could be oxidized prior to metal binding, rendering them unable to bind zinc and fold, also permanently exposing the MqsA degron following synthesis (Fig. 6). Both scenarios would render the MqsA degron accessible for binding. Consistent with this possibility, MqsA protein has been shown, *in vivo*, to be degraded under oxidative conditions (10, 21) (exposure to H_2O_2, a chemical that readily oxidizes cysteines). Because H_2O_2 fails to oxidize metal-loaded MqsA (the zinc-coordinating cysteine residues are protected from oxidation by the bound zinc), this leads to a model in which only actively translated and nascent MqsA is the predominant target. Similarly, synthesized toxin-free YefM or nascent YefM is the only YefM species targeted for degradation.

Whether this results in the activation of MqsR depends on the extent of the exposure to the stress. Prior to recent work, including this study, the prevailing model for toxin activation had been that stress results in the selective degradation of antitoxins within a TA complex, "freeing" the toxin to exert its toxic activities and arrest cell growth (1, 4). However, our data, and that of others, have shown this model is incorrect as toxins bound to their cognate antitoxins clearly inhibit antitoxin degradation (10). Thus, while stress results in the selective degradation of free and nascent and/or unfolded antitoxins, it does not result in the degradation of antitoxins present in TA complexes. Therefore, the antitoxin-bound toxins will never become "free" to exert their toxic effects. However, despite this discovery, this does not mean toxins are never active. Namely, when toxin concentrations exceed those of their cognate antitoxins, the excess cellular toxins will be free to act on their endogenous substrates, and, in turn, inhibit cell growth.

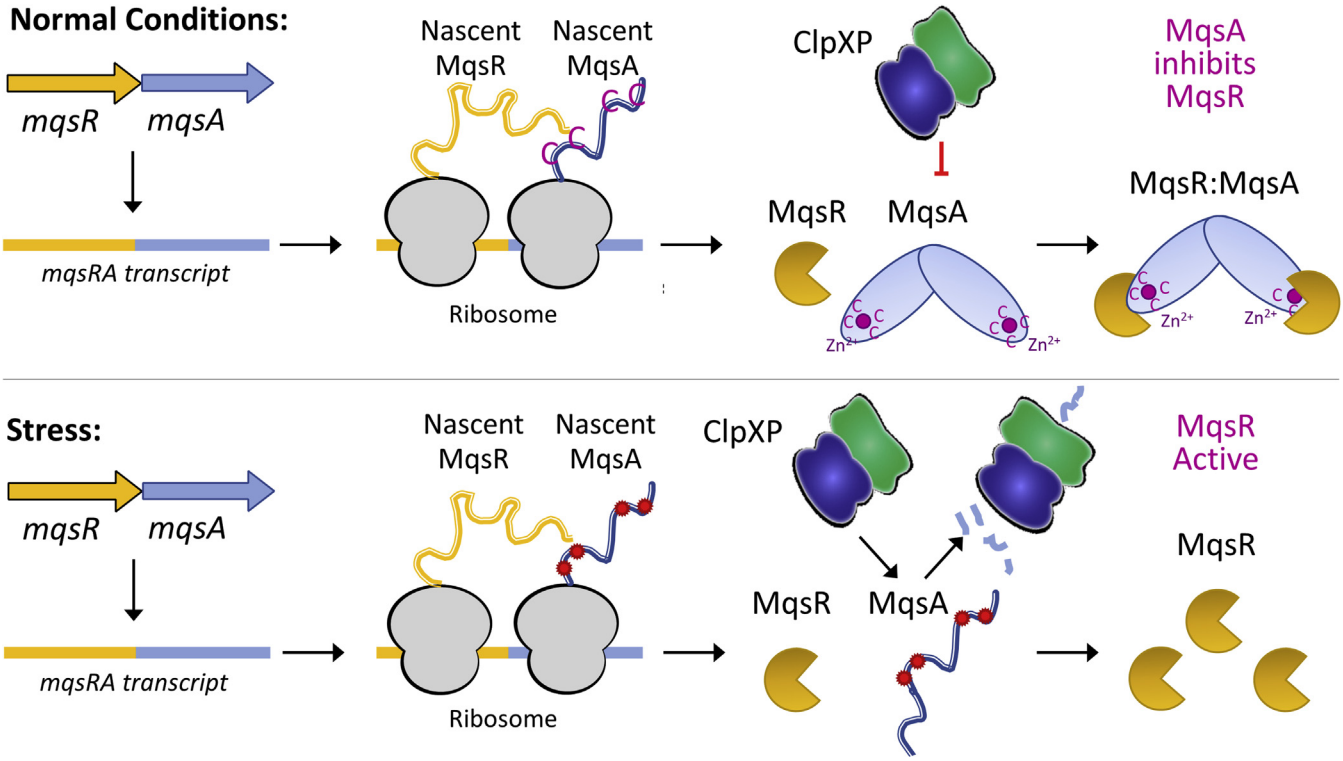

Figure 6. Model of MqsA degradation by ClpXP and activation of the MqsR toxin. Under normal conditions (*top*), both MqsA and MqsR are translated and folded, leading to complex formation and toxin inhibition. Under stress conditions, MqsR folds, whereas MqsA does not (MqsA$_u$), for example, because of oxidation of the four cysteine residues that coordinate zinc. This exposes a cryptic ClpX$_N$-binding motif on MqsA, resulting in ClpX$_N$ binding and ClpXP-mediated degradation. MqsR is then free to cleave its mRNA substrates, ultimately resulting in growth arrest.

Antitoxin degradation potently activates TA operon transcription. In most cases, this results in sufficient expression of antitoxin to match or exceed the concentration of toxin (Fig. 6). However, it is possible that extended exposure to stress may cause this balance to shift, resulting in excess toxin and growth arrest (Fig. 6). For example, although it is established that MqsA transcription and expression exceeds that of MqsR, if all newly synthesized MqsA is degraded, eventually the newly synthesized MqsR will not have a cognate antitoxin available for binding, allowing it to target and cleave its endogenous substrate GCU/A mRNA sequences. The endogenous environmental stressors (and the extent to which they must be exposed) that ultimately activate MqsR *via* MqsA degradation, and other TA systems, as well as regulated proteolysis by other proteases, such as Lon, are still active areas of investigation.

Experimental procedures

Cloning, expression, and purification

$MqsA_N$ and $ClpX_N$ were subcloned in the RP1B vector, containing a cleavable N-terminal hexahistidine (His_6) tag followed by a tobacco etch virus (TEV) cleavage sequence. To facilitate stable expression, $MqsA_{1-34}$ was subcloned into the pTHMT vector, which includes an N-terminal maltose-binding protein followed by a TEV cleavage sequence. Mutagenesis was carried out using the QuikChange Mutagenesis Kit (Agilent Technologies) using the manufacturer's protocols; all constructs were verified by sequencing. For expression, plasmid DNAs were transformed into *E. coli* BL21(λDE3) cells. Cells were grown with shaking at 37 °C in either LB for nonlabeled proteins or M9 minimal media containing 1 g/l of $^{15}NH_4Cl$ and 4 g/l of D-glucose as the sole nitrogen and carbon sources, respectively, with appropriate antibiotics. Once the cultures reached an absorbance of ∼0.8 at 600 nm, they were cooled at 4 °C for 1 h, 1 mM IPTG was added to induce expression, and the cultures were transferred to 18 °C for 18 h with shaking. Cells were harvested by centrifugation at 8000*g* for 10 min, and pellets were stored at −80 °C.

$MqsA_N$ was purified as previously described (11). Briefly, cell pellets were resuspended in lysis buffer (50 mM Tris–HCl, pH 8.0, 500 mM NaCl, 5 mM imidazole, 0.1% Triton X-100, and EDTA-free protease inhibitor), lysed by high-pressure cell homogenization (Avestin C3-Emulsiflex), and the cell debris was pelleted by centrifugation (42,000*g*, 45 min). The supernatant was filtered with 0.22 μm syringe filters, loaded onto a HisTrap HP column pre-equilibrated with buffer A (50 mM Tris, pH 8.0, 500 mM NaCl, and 5 mM imidazole), and eluted using a linear gradient of buffer B (50 mM Tris, pH 8.0, 500 mM NaCl, and 500 mM imidazole). Fractions containing $MqsA_N$ were pooled and dialyzed overnight at 4 °C with TEV protease to cleave the His_6 tag. The cleaved protein was incubated with Ni^{2+}–NTA resin (GE Healthcare), and the flow-through was collected. The protein was concentrated and purified using SEC (Superdex 75 26/60 [GE Healthcare]) pre-equilibrated with NMR buffer 1 (20 mM Na/PO_4, pH 6.5, 50 mM NaCl, and 0.5 mM Tris(2-carboxyethyl)phosphine [TCEP]). $ClpX_N$ and $MqsA_{1-34}$ were purified similarly but with the following differences. The $ClpX_N$ sizing buffer included 0.5 mM $ZnSO_4$ (20 mM Na/PO_4, pH 6.5, 50 mM NaCl, 0.5 mM TCEP, and 0.5 mM $ZnSO_4$). Prior to SEC, the $MqsA_{1-34}$ was heat purified twice by incubating the sample at 80 °C for 10 min. The sample was then centrifuged at 15,000*g* for 10 min to remove precipitated protein, concentrated, and purified using SEC (Superdex 75 26/60) in NMR buffer.

MqsR was also purified as described previously (39). Briefly free and folded MqsR is obtained by coexpressing pET30a-MqsR (which includes an N-terminal His6 tag), with untagged pCA21a-$MqsA_N$ I44A ($MqsA_N$ is the N-terminal domain of MqsA and includes residues 1–76) at 18 °C in BL21(DE3) *E. coli* competent cells. After lysis, the His_6-MqsR–$MqsA_N$ complex was bound to nickel metal affinity resin and denatured with 6 M guanidine hydrochloride. His_6-MqsR (hereafter referred to as MqsR) was eluted with 500 mM imidazole and refolded by stepwise dialysis in buffers containing decreasing amounts of guanidine hydrochloride followed by a final preparative gel filtration step (Superdex 75 16/60; GE Healthcare; SEC buffer, 10 mM Tris, pH 7.5, 50 or 100 mM NaCl, and 0.5 mM TCEP).

To construct Gfp-$MqsA_{1-34}$, genes encoding Gfp and MqsA were cloned into pBad24 (40), a stop codon was introduced by site-directed mutagenesis at codon 35 of *mqsA*, and mutagenesis was confirmed by direct sequencing. Gfp-$MqsA_{1-34}$ expression was induced in log phase *E. coli* BL21(λDE3) Δ*clpP*::*cat* cells with arabinose (0.2%) for 6 h by shaking at 25 °C. Cells were harvested, lysed by French press, and Gfp-$MqsA_{1-34}$ was purified from soluble cell lysates by organic extraction and phenyl Sepharose chromatography as described (41). Gfp-ssrA, ClpX, and ClpP were overexpressed in *E. coli* BL21(λDE3) and purified as previously described (32, 41–43). ClpX N-domain mutations were introduced into pET-ClpX by site-directed mutagenesis, confirmed by direct sequencing, and purified as WT ClpX. ClpX WT and N-domain variants were fractionated on Sephacryl S-200 HR (GE Healthcare), and hexamers were collected. To confirm enzymatic activity, ATP hydrolysis was monitored by measuring phosphate release with Biomol green reagent (Enzo Life Sciences) in reactions containing ClpX WT and mutant proteins (0.5 μM) and ATP (5 mM) in 50 mM Hepes, pH 7.5, 150 mM KCl, and 20 mM $MgCl_2$, at 23 °C. A C-terminal SspB peptide (NH_2-RGGRPALRVVK-COOH) was synthesized and purchased from Life Technologies. Protein concentrations are reported as Gfp monomers, ClpX hexamers, and ClpP tetradecamers.

Preparation of metal-free MqsA for degradation experiments

Purified MqsA constructs were diluted to 10 μM in the presence of 10 mM EDTA, heated for 10 min at 80 °C, and then allowed to cool to room temperature for 5 min. Samples were then dialyzed against 10 mM Tris–HCl, pH 7.0, 50 mM NaCl, and 0.5 mM TCEP overnight at 4 °C. Prior to freezing, the samples were centrifuged at 15,000*g* for 10 min at 4 °C to remove any precipitated protein.

Sequence-specific backbone assignment

^{15}N, ^{13}C-labeled $MqsA_{1-34}$ (85 μM; concentrations greater than 100 μM precipitated) and ^{15}N, ^{13}C-labeled $MqsA_N$ (650 μM) were prepared in NMR buffer 1, whereas ^{15}N, ^{13}C-labeled $ClpX_N$ (800 μM) was prepared in NMR buffer containing 0.5 mM $ZnSO_4$; 10% (v/v) D_2O was added immediately prior to data acquisition. The sequence-specific backbone assignments of $ClpX_N$, $MqsA_N$, and $MqsA_{1-34}$ were determined by recording a suite of heteronuclear NMR spectra including: 2D [^1H, ^{15}N] HSQC, 3D HNCA, 3D HN(CO)CA, 3D HNCACB, and 3D CBCA(CO)NH. For $ClpX_N$, the sequence-specific backbone assignments were verified and expanded using a 3D HNCO, 3D HN(CA)CO, and 3D (H)CC(CO)NH. All NMR data were collected on a Bruker Advance Neo 600 MHz Spectrometer and an 800 MHz Spectrometer equipped with TCI HCN z-gradient cryoprobe at 298 K. Data were processed using Topspin (Bruker) and analyzed using CARA (http://www.cara.nmr.ch) and CCPN (44, 45). To test the role of zinc for $ClpX_N$ spectrum quality, ^{15}N-labeled $ClpX_N$ (200 μM) was purified as described with the exception that the NMR buffer did not contain $ZnSO_4$. After recording a 2D [^1H, ^{15}N] HSQC spectrum, 500 μM $ZnSO_4$ was added, and a 2D [^1H, ^{15}N] HSQC spectrum was recorded and a direct comparison performed.

MqsA-$ClpX_N$ NMR spectroscopy interaction studies

All NMR data were collected on a Bruker Advance Neo 600 MHz Spectrometer equipped with TCI HCN z-gradient cryoprobe at 298 K. $MqsA_N$, $MqsA_{1-34}$, and $ClpX_N$ were purified in NMR buffer containing 0.5 mM $ZnSO_4$. $MqsA_N$ was titrated into ^{15}N-labeled $ClpX_N$ (50 μM) in molar ratios of 1:1, 1:2, 1:5, and 1:10 and 2D [^1H, ^{15}N] HSQC spectra were recorded, resulting in no observable interaction. $MqsA_{1-34}$ was titrated into ^{15}N-labeled $ClpX_N$ (50 μM) in ratios of 1:1, 1:2, 1:4, and 1:8, with 2D [^1H, ^{15}N] HSQC spectra recorded for each sample. These titrations were used to follow CSPs in $ClpX_N$ upon binding; the majority of peaks are in the fast exchange regime and thus can be readily traced. $ClpX_N$ was titrated into ^{15}N-labeled $MqsA_{1-34}$ in ratios of 1:0.5, 1:1, 1:2, and 1:4 with 2D [^1H, ^{15}N] HSQC spectra recorded for each sample. These titrations were used to follow CSPs in $MqsA_{1-34}$; all peaks are in the fast exchange regime and thus can be readily traced. Chemical shift differences (Δδ) were calculated using the following equation:

$$\Delta\delta(p.p.m.) = \sqrt{(\Delta\delta_H)^2 + \left(\frac{\Delta\delta_N}{5}\right)^2}$$

Proteolysis and direct binding assays

$MqsA_{FL}$, $MqsA_{FLmf}$, $MqsA_N$, or $MqsA_{Nmf}$ (6 μM) was incubated with ClpX (1 μM) and ClpP (1 μM), or as indicated, in 50 mM Mes buffer, pH 6.5, 110 mM KCl, 20 mM $MgCl_2$, 5 mM ATP, and acetate kinase (25 μg ml^{-1}) (Sigma–Aldrich) and 15 mM acetyl phosphate (Sigma–Aldrich) at 23 °C. At the indicated times, samples were removed, and reactions were analyzed by SDS-PAGE and Coomassie staining. Where indicated, purified MqsR (10 μM) and SspB peptide (150 μM) were included in the degradation reactions. To monitor degradation by loss of fluorescence, Gfp-$MqsA_{1-34}$ (0.5 μM) was incubated with ClpX (0.75 μM) and ClpP (1.2 μM) in degradation buffer (50 mM Hepes, pH 7.0, 100 mM KCl, 20 mM $MgCl_2$, 0.005% Triton X-100, 5 mM ATP, 25 μg/ml acetate kinase, and 15 mM acetyl phosphate) at 23 °C. Fluorescence was monitored using an Agilent Eclipse spectrofluorometer at excitation and emission wavelengths of 420 and 510 nm, respectively.

To detect substrate binding, ClpX WT and N-domain variants (0.7 μM) were incubated with ClpP (1.4 μM) and Gfp-$MqsA_{1-34}$ (3 μM) in substrate binding buffer (50 mM Hepes, pH 7.0, 100 mM KCl, 10 mM $MgCl_2$, 0.004% Triton X-100, 50 μg/ml bovine serum albumin, and 5 mM ATP) on ice for 15 min. Stable complexes were collected by centrifugation at 20,000*g* for 20 min and retained on a Nanosep polyethersulfone filter (Pall) with a molecular weight cutoff of 100 kDa. Retained complexes were collected, and substrate was quantified by fluorescence.

Antibiotic chase assays

The pBAD24 vector encoding Gfp-$MqsA_{1-34}$ was transformed into MG1655 WT and MG1655 *ΔclpPX*::kan strains. Overnight cultures were grown and back-diluted the following day to an absorbance of 0.05 at 600 nm in a 30 ml culture. Ampicillin (100 μg/ml) and L-arabinose (0.01%) were added, and cultures were grown at 37 °C until reaching an absorbance of 0.7 at 600 nm. Spectinomycin (200 μg/ml) was added to the cultures to stop protein synthesis, and cells were collected at 0, 5, 10, 15, and 30 min. Total cellular proteins were immediately precipitated with trichloroacetic acid (Sigma) (15% v/v) as described (32). Protein turnover was monitored by Western blot using anti-Gfp rabbit IgG (Invitrogen), Horseradish peroxidase–linked anti-rabbit IgG (Cell Signaling Technology) and chemiluminescence (Pierce ECL Western Blotting Substrate; Thermo Fisher Scientific). Band intensity was quantified by densitometry (ImageJ, the National Institutes of Health).

Data availability

NMR chemical shifts have been deposited in the Biological Magnetic Resonance Data Bank (BioMagResBank or BMRB: 50781, 50782, and 50784).

Supporting information—This article contains supporting information.

Acknowledgments—We thank Victor Yu and Dr Eric Ronzone for preparation of metal-free MqsA.

Author contributions—W. P., J. L. C., and R. P. conceptualization; M. R. V., W. P., J. L. C., and R. P. methodology; B. P., C. J. L., N. R., C. E. T., W. P., J. L. C., and R. P. validation; M. R. V., C. J. L., N. R., C. E. T., W. P., J. L. C., and R. P. formal analysis; M. R. V., B. P., C. J. L., N. R., C. E. T., M. S., W. P., and J. L. C. investigation; W. P. and J. L. C. data curation; M. R. V., J .L. C., and R. P. writing–original draft; M. R. V., B. P., C. J. L., W. P., and R. P.

writing–review & editing; N. R. visualization; W. P., J. L. C., and R. P. supervision; W. P., J. L. C., and R. P. project administration; J. L. C. and R. P. funding acquisition.

Funding and additional information—This work was supported by the National Science Foundation grant MCB-1817621 (to J. L. C. and R. P.) and the National Science Foundation Graduate Research Fellowship Program (DGE-2136520 to M. R. V.).

Conflict of interest—The authors declare that they have no conflicts of interest with the contents of this article.

Abbreviations—The abbreviations used are: CSP, chemical shift perturbation; Gfp-ssrA, Gfp fused to the ssrA tag sequence; His6, hexahistidine tag; HSQC, heteronuclear single quantum coherence; IDP, intrinsically disordered protein; $MqsA_C$, C-terminal domain of MqsA; $MqsA_N$, N-terminal domain of MqsA; $MqsA_{FL}$, full-length MqsA; $MqsA_{FL}{}_{mf}$, metal-free MqsA; SEC, size-exclusion chromatography; TA, toxin–antitoxin; TCEP, Tris(2-carboxyethyl)phosphine; TEV, tobacco etch virus.

References

1. Page, R., and Peti, W. (2016) Toxin-antitoxin systems in bacterial growth arrest and persistence. *Nat. Chem. Biol.* **12**, 208–214
2. Gerdes, K., Rasmussen, P. B., and Molin, S. (1986) Unique type of plasmid maintenance function: Postsegregational killing of plasmid-free cells. *Proc. Natl. Acad. Sci. U. S. A.* **83**, 3116–3120
3. Gotfredsen, M., and Gerdes, K. (1998) The Escherichia coli relBE genes belong to a new toxin-antitoxin gene family. *Mol. Microbiol.* **29**, 1065–1076
4. Maisonneuve, E., and Gerdes, K. (2014) Molecular mechanisms underlying bacterial persisters. *Cell* **157**, 539–548
5. Keren, I., Shah, D., Spoering, A., Kaldalu, N., and Lewis, K. (2004) Specialized persister cells and the mechanism of multidrug tolerance in Escherichia coli. *J. Bacteriol.* **186**, 8172–8180
6. Moyed, H. S., and Bertrand, K. P. (1983) hipA, a newly recognized gene of Escherichia coli K-12 that affects frequency of persistence after inhibition of murein synthesis. *J. Bacteriol.* **155**, 768–775
7. Cheverton, A. M., Gollan, B., Przydacz, M., Wong, C. T., Mylona, A., Hare, S. A., and Helaine, S. (2016) A Salmonella toxin promotes persister formation through acetylation of tRNA. *Mol. Cell* **63**, 86–96
8. Goormaghtigh, F., Fraikin, N., Putrinš, M., Hallaert, T., Hauryliuk, V., Garcia-Pino, A., Sjödin, A., Kasvandik, S., Udekwu, K., Tenson, T., Kaldalu, N., and Van Melderen, L. (2018) Reassessing the role of type II toxin-antitoxin systems in formation of Escherichia coli type II persister cells. *mBio* **9**, e00640-18
9. Holden, D. W., and Errington, J. (2018) Type II toxin-antitoxin systems and persister cells. *mBio* **9**, e01574-18
10. LeRoux, M., Culviner, P. H., Liu, Y. J., Littlehale, M. L., and Laub, M. T. (2020) Stress can induce transcription of toxin-antitoxin systems without activating toxin. *Mol. Cell* **79**, 280–292.e8
11. Brown, B. L., Grigoriu, S., Kim, Y., Arruda, J. M., Davenport, A., Wood, T. K., Peti, W., and Page, R. (2009) Three dimensional structure of the MqsR:MqsA complex: A novel TA pair comprised of a toxin homologous to RelE and an antitoxin with unique properties. *PLoS Pathog.* **5**, e1000706
12. Garcia-Pino, A., Balasubramanian, S., Wyns, L., Gazit, E., De Greve, H., Magnuson, R. D., Charlier, D., van Nuland, N. A. J., and Loris, R. (2010) Allostery and intrinsic disorder mediate transcription regulation by conditional cooperativity. *Cell* **142**, 101–111
13. Castro-Roa, D., Garcia-Pino, A., De Gieter, S., van Nuland, N. A. J., Loris, R., and Zenkin, N. (2013) The Fic protein Doc uses an inverted substrate to phosphorylate and inactivate EF-Tu. *Nat. Chem. Biol.* **9**, 811–817
14. Christensen, S. K., Maenhaut-Michel, G., Mine, N., Gottesman, S., Gerdes, K., and Van Melderen, L. (2004) Overproduction of the Lon protease triggers inhibition of translation in Escherichia coli: Involvement of the yefM-yoeB toxin-antitoxin system. *Mol. Microbiol.* **51**, 1705–1717
15. Van Melderen, L., Bernard, P., and Couturier, M. (1994) Lon-dependent proteolysis of CcdA is the key control for activation of CcdB in plasmid-free segregant bacteria. *Mol. Microbiol.* **11**, 1151–1157
16. Fraikin, N., Rousseau, C. J., Goeders, N., and Van Melderen, L. (2019) Reassessing the role of the type II MqsRA toxin-antitoxin system in stress response and biofilm formation: mqsA is transcriptionally uncoupled from mqsR. *mBio* **10**, e02678-19
17. Overgaard, M., Borch, J., and Gerdes, K. (2009) RelB and RelE of Escherichia coli form a tight complex that represses transcription via the ribbon-helix-helix motif in RelB. *J. Mol. Biol.* **394**, 183–196
18. Prysak, M. H., Mozdzierz, C. J., Cook, A. M., Zhu, L., Zhang, Y., Inouye, M., and Woychik, N. A. (2009) Bacterial toxin YafQ is an endoribonuclease that associates with the ribosome and blocks translation elongation through sequence-specific and frame-dependent mRNA cleavage. *Mol. Microbiol.* **71**, 1071–1087
19. Dubiel, A., Wegrzyn, K., Kupinski, A. P., and Konieczny, I. (2018) ClpAP protease is a universal factor that activates the parDE toxin-antitoxin system from a broad host range RK2 plasmid. *Sci. Rep.* **8**, 15287
20. Ruangprasert, A., Maehigashi, T., Miles, S. J., and Dunham, C. M. (2017) Importance of the *E. coli* DinJ antitoxin carboxy terminus for toxin suppression and regulated proteolysis: Functional characterization of the *E. coli* DinJ-YafQ complex. *Mol. Microbiol.* **104**, 65–77
21. Wang, X., Kim, Y., Hong, S. H., Ma, Q., Brown, B. L., Pu, M., Tarone, A. M., Benedik, M. J., Peti, W., Page, R., and Wood, T. K. (2011) Antitoxin MqsA helps mediate the bacterial general stress response. *Nat. Chem. Biol.* **7**, 359–366
22. Christensen-Dalsgaard, M., Jørgensen, M. G., and Gerdes, K. (2010) Three new RelE-homologous mRNA interferases of Escherichia coli differentially induced by environmental stresses. *Mol. Microbiol.* **75**, 333–348
23. Yamaguchi, Y., Park, J. H., and Inouye, M. (2009) MqsR, a crucial regulator for quorum sensing and biofilm formation, is a GCU-specific mRNA interferase in Escheichia coli. *J. Biol. Chem.* **284**, 28746–28753
24. Brown, B. L., Wood, T. K., Peti, W., and Page, R. (2011) Structure of the Escherichia coli antitoxin MqsA (YgiT/b3021) bound to its gene promoter reveals extensive domain rearrangements and the specificity of transcriptional regulation. *J. Biol. Chem.* **286**, 2285–2296
25. Sauer, R. T., and Baker, T. A. (2011) AAA+ proteases: ATP-fueled machines of protein destruction. *Annu. Rev. Biochem.* **80**, 587–612
26. Olivares, A. O., Baker, T. A., and Sauer, R. T. (2018) Mechanical protein unfolding and degradation. *Annu. Rev. Physiol.* **80**, 413–429
27. Park, E. Y., Lee, B.-G., Hong, S.-B., Kim, H.-W., Jeon, H., and Song, H. K. (2007) Structural basis of SspB-tail recognition by the zinc binding domain of ClpX. *J. Mol. Biol.* **367**, 514–526
28. Neher, S. B., Sauer, R. T., and Baker, T. A. (2003) Distinct peptide signals in the UmuD and UmuD' subunits of UmuD/D' mediate tethering and substrate processing by the ClpXP protease. *Proc. Natl. Acad. Sci. U. S. A.* **100**, 13219–13224
29. Gonzalez, M., Rasulova, F., Maurizi, M. R., and Woodgate, R. (2000) Subunit-specific degradation of the UmuD/D' heterodimer by the ClpXP protease: The role of trans recognition in UmuD' stability. *EMBO J.* **19**, 5251–5258
30. Wojtyra, U. A., Thibault, G., Tuite, A., and Houry, W. A. (2003) The N-terminal zinc binding domain of ClpX is a dimerization domain that modulates the chaperone function. *J. Biol. Chem.* **278**, 48981–48990
31. Abdelhakim, A. H., Oakes, E. C., Sauer, R. T., and Baker, T. A. (2008) Unique contacts direct high-priority recognition of the tetrameric Mu transposase-DNA complex by the AAA+ unfoldase ClpX. *Mol. Cell* **30**, 39–50
32. Camberg, J. L., Hoskins, J. R., and Wickner, S. (2009) ClpXP protease degrades the cytoskeletal protein, FtsZ, and modulates FtsZ polymer dynamics. *Proc. Natl. Acad. Sci. U. S. A.* **106**, 10614–10619

33. Donaldson, L. W., Wojtyra, U., and Houry, W. A. (2003) Solution structure of the dimeric zinc binding domain of the chaperone ClpX. *J. Biol. Chem.* **278**, 48991–48996
34. Papadopoulos, E., Collet, J.-F., Vukojević, V., Billeter, M., Holmgren, A., Gräslund, A., and Vlamis-Gardikas, A. (2012) Solution structure and biophysical properties of MqsA, a Zn-containing antitoxin from Escherichia coli. *Biochim. Biophys. Acta* **1824**, 1401–1408
35. Viola, M. G., LaBreck, C. J., Conti, J., and Camberg, J. L. (2017) Proteolysis-dependent remodeling of the tubulin homolog FtsZ at the division septum in Escherichia coli. *PLoS One* **12**, e0170505
36. Wah, D. A., Levchenko, I., Rieckhof, G. E., Bolon, D. N., Baker, T. A., and Sauer, R. T. (2003) Flexible linkers leash the substrate binding domain of SspB to a peptide module that stabilizes delivery complexes with the AAA+ ClpXP protease. *Mol. Cell* **12**, 355–363
37. Kim, Y., Wang, X., Zhang, X.-S., Grigoriu, S., Page, R., Peti, W., and Wood, T. K. (2010) Escherichia coli toxin/antitoxin pair MqsR/MqsA regulate toxin CspD. *Environ. Microbiol.* **12**, 1105–1121
38. Flynn, J. M., Neher, S. B., Kim, Y. I., Sauer, R. T., and Baker, T. A. (2003) Proteomic discovery of cellular substrates of the ClpXP protease reveals five classes of ClpX-recognition signals. *Mol. Cell* **11**, 671–683
39. Brown, B. L., Lord, D. M., Grigoriu, S., Peti, W., and Page, R. (2013) The Escherichia coli toxin MqsR destabilizes the transcriptional repression complex formed between the antitoxin MqsA and the mqsRA operon promoter. *J. Biol. Chem.* **288**, 1286–1294
40. Guzman, L. M., Belin, D., Carson, M. J., and Beckwith, J. (1995) Tight regulation, modulation, and high-level expression by vectors containing the arabinose PBAD promoter. *J. Bacteriol.* **177**, 4121–4130
41. Yakhnin, A. V., Vinokurov, L. M., Surin, A. K., and Alakhov, Y. B. (1998) Green fluorescent protein purification by organic extraction. *Protein Expr. Purif.* **14**, 382–386
42. Maurizi, M. R., Thompson, M. W., Singh, S. K., and Kim, S. H. (1994) Endopeptidase Clp: ATP-dependent Clp protease from Escherichia coli. *Methods Enzymol.* **244**, 314–331
43. Grimaud, R., Kessel, M., Beuron, F., Steven, A. C., and Maurizi, M. R. (1998) Enzymatic and structural similarities between the Escherichia coli ATP-dependent proteases, ClpXP and ClpAP. *J. Biol. Chem.* **273**, 12476–12481
44. Mureddu, L., and Vuister, G. W. (2019) Simple high-resolution NMR spectroscopy as a tool in molecular biology. *FEBS J.* **286**, 2035–2042
45. Vranken, W. F., Boucher, W., Stevens, T. J., Fogh, R. H., Pajon, A., Llinas, M., Ulrich, E. L., Markley, J. L., Ionides, J., and Laue, E. D. (2005) The CCPN data model for NMR spectroscopy: Development of a software pipeline. *Proteins* **59**, 687–696